Environment, Development and Sustainability
https://doi.org/10.1007/s10668-022-02264-z

Spatialization of Chinese R-410A emissions from the room air-conditioning sector

Pengcheng Wu[1,2] · Li Zhang[2,3] · Bo Yao[4] · Bofeng Cai[2] · Yifang Zhu[3] · Hui Liu[5] · Pengling Wang[6] · Lisha Liu[7] · Yanwei Dou[8] · Han Yan[9] · Yijun Liu[10] · Zixuan Xie[11] · Lingyun Pang[2] · Libin Cao[2] · Yimeng Ren[12] · Xin Bo[13]

Received: 18 October 2021 / Accepted: 4 March 2022
© The Author(s), under exclusive licence to Springer Nature B.V. 2022

Abstract
Hydrofluorocarbons (HFCs) are strong greenhouse gases and regulated by the Montreal Protocol as substitutes of ozone depletion substances. Currently, Chinese HFC emissions keep increasing, and the inventory is only on a national or city level. A high-resolution gridded HFC emission inventory is needed to develop HFC reduction policy and phase-down schedule. We developed a method by integrating point sources with longitude and latitude information and area sources using the proxy factor to explore the distribution of R-410A [a mixture of HFC-32 (CH_2F_2) and HFC-125 (C_2HF_5)] emissions from the room air-conditioning sector on a 10×10 km^2 grid scale. Variety of regression models (including the principal component analysis, multiple linear regressions, stepwise regressions, and linear regression), analysis scale (national level and provincial level), and data dimensions (the proxy factor and unit-area value) were tested. The gross domestic product was found as the optimal proxy factor and used to spatialize R-410A emissions at a high-resolution scale. Compared to the national-level analysis, model evaluation parameters were largely improved for the provincial-level regression analysis, including root-mean-square error (from 20.96 to 11.35), normalized mean bias (from 0.16 to −0.01), normalized mean error (from 0.45 to 0.20), mean absolute error (from 11.27 to 4.97), correlation coefficient (from 0.91 to 0.97), and relative error (from 39% to 76%), suggesting a better performance for the provincial-level analysis. This study provides a cost-effective method to establish fine-resolution HFC inventory. Meanwhile, high-resolution emissions grid data could be further applied to implement site-specific management of low-carbon development.

Keywords High-resolution · R-410A emissions · Hydrofluorocarbons · Room air-conditioning · Spatialization · Proxy factors

Pengcheng Wu and Li Zhang contributed equally to this work

✉ Bo Yao
yaobo@fudan.edu.cn

✉ Bofeng Cai
caibf@caep.org.cn

✉ Yifang Zhu
yifang@ucla.edu

Extended author information available on the last page of the article

Published online: 02 April 2022

Abbreviations

AAT	Average annual temperature
HDD18 & CDD26	Heating degree days and cooling degree days
CO_2-eq	Carbon dioxide-equivalent
DMSP-OLS	Defense Meteorological Satellite Program Operational Linescan System
F-gas	Fluorinated greenhouse gas
GDP	Gross domestic product
GHG	Greenhouse gas
GWP	Global warming potential
HFC	Hydrofluorocarbon
R-410A	Known as HFC-410A, a blend of HFC-32 (CH_2F_2) and HFC-125 (C_2HF_5)
NTL	Nighttime light
ODS	Ozone-depleting substance
RAC	Room air-conditioning
RP	Resident population

List of symbols

$E_{Inventory,i}$	R-410A emissions of the prefecture-level city i from emission inventory (kg)
$E_{model,i}$	R-410A emissions of the prefecture-level city i from the model prediction (kg)
$GDP_{grid,j}$	GDP value in each of the 10×10 km^2 grid of the province or a province-level municipality j (10^{10} RMB)
$GDP_{province,j}$	Summed GDP value of the province or a province-level municipality j (10^{10} RMB)
$HFC-410A_{grid,j}$	R-410A emissions in each of the 10×10 km^2 grid of the province or a province-level municipality j (kg)
$HFC-410A_{province,j}$	Total R-410A emissions of the province or a province-level municipality j (kg)
N	Number of prefecture-level cities, $N=330$
NMB	Normalized mean bias
NME	Normalized mean error
MAE	Mean absolute error
R	Correlation coefficient
RE	Relative error
$RMSE$	Root-mean-square error

1 Introduction

Climate change causes adverse effects in meteorological events resulting from global warming, which is closely related to human activities (De Matteis, 2017; Yilmaz & Can, 2019). The Paris Agreement that was adopted at the Paris Climate Change Conference in December 2015 requires the participating countries to reach the goal of zero carbon emissions by the second half of the twenty-first century (UNFCCC, 2015). The goal showed the determination of global cooperation and established higher requirements

for reducing greenhouse gas (GHG) emissions worldwide to collectively tackle climate change (Gao et al., 2017). A report by the Netherlands Environmental Assessment Agency (Olivier et al., 2018) indicated that in 2017 global GHG emissions were increasing at a rate of 1.3%, reaching 50.9 Gt CO_2 equivalent (CO_2-eq). Specifically, fluorinated greenhouse gas (F-gas) emissions increased by an annual average of 5.6% during 2004–2014. F-gas emissions contributed about 3% of global GHG emissions (not including those caused by land-use changes). In the USA, although a decreasing trend was observed for GHG emissions, F-gas emissions increased by about 69.7% between 1990 and 2017 (US EPA, 2021). In China, the GHG emissions increased from 8.0 Gt CO_2-eq in 2005 to 12.3 Gt CO_2-eq in 2014 (not including those caused by land use, land-use change, and forestry), in which the contribution of F-gas increased from 1.6% (0.13 Gt CO_2-eq) in 2005 to 2.4% (0.30 Gt CO_2-eq) in 2014, and 90% of the F-gas emissions are from hydrofluorocarbons (HFCs) (China Ministry of Ecology & Environment, 2018).

In compliance with the Montreal Protocol to control the consumption and production of ozone-depleting substances (ODSs), manufacturers have widely adopted HFCs to replace chlorofluorocarbons, halons, and hydrochlorofluorocarbons in refrigeration, air-conditioning, foam blowing, fire protection, and other applications since the 1990s due to their negligible effect on stratospheric ozone loss (World Meteorological Organization, 2018). However, most HFCs are potent GHGs with high global warming potentials (GWPs). Thus, the abundances of most HFCs are increasing in the global atmosphere. Specifically, HFC emissions increased by 23% from 2012 to 2016 and contributed to 1.5% of total GHG emissions as carbon dioxide-equivalent emissions (CO_2-eq) (World Meteorological Organization, 2018). It is projected that the global HFC will account for 9–19% of total GHG emissions as CO_2-eq by 2050 under the "business-as-usual" scenario (Velders et al., 2009). Therefore, goals for reducing the production and consumption of HFCs in both developed and developing countries were set up by the Kigali Amendment to the Montreal Protocol in 2016 (UNEP, 2016). China, for instance, contributed to 24% of global ODSs and HFC emissions in 2014, mainly due to widely used HFC as refrigerants (Fang et al., 2018). It is projected that China's HFC emissions will increase substantially in 2050 if not regulated (Fang et al., 2016; Velders et al., 2015). Therefore, it is important that China should implement comprehensive policies and strategies to manage HFC emissions.

A high-resolution gridded HFC emission inventory is necessary to provide pertinent emission reduction guidance for the local government in establishing policies. The database can also be used as a prior emission for inverse modeling to quantify GHG emissions at a fine resolution. However, HFC emissions data are difficult to obtain since they are closely related to the dynamic processes of refrigerants used in refrigerators and air-conditioners. Previous studies on HFC emissions in China have been conducted at the national level (Fang et al., 2018; Wan et al., 2009, 2016), and only limited studies of HFC species have been conducted at the city level (Liu et al., 2019; Su et al., 2015). Considering the fact that both HFC and CO_2 emissions include emission from point source and area sources, and the CO_2 emission inventory has been spatialized from the national level, or city level, or at a high-resolution level with a spatial resolution of 1×1 km^2 or 10×10 km^2. These CO_2 spatialization methods can be used as a reference for HFC (Cai, 2014; Cai et al. 2017; Wang et al., 2014). Based on the high-resolution CO_2 data, various policy suggestions have been proposed, including establishing city-level responsibility for emission reduction when allocating the national goal and conducting benchmark research studies. In order to depict high-resolution CO_2 emissions, proper proxy factors, including resident population (RP) data (Cai & Zhang, 2014), nighttime light (NTL) data (Oda & Maksyutov, 2011), have

been identified. Thus, it is necessary to find the proper proxy factors to develop high-resolution HFC emissions as well.

In this study, R-410A, also known as HFC-410A (a blend of HFC-32 (CH_2F_2) and HFC-125 (C_2HF_5) that are two of the main contributors to the total HFC emissions), from the room air-conditioning (RAC) sector were chosen (Fang et al., 2016; Liu et al., 2019). The prefecture-level R-410A emissions data from the RAC in 2015, combined with proxy factors, were analyzed to explore the distribution of R-410A emissions on a 10×10 km^2 grid scale. To the best of our knowledge, this is the first study to spatialize specific HFC emissions at a high-resolution scale. The results of this study may provide practical guidance on future policies in reducing the R-410A and other F-gas emissions in China. The developed method that uses provincial-level regression analysis based on proxy factor gross domestic product (GDP) could also be applied to other countries or regions in the spatialization of R-410A emissions where activity data or emission factors are difficult to obtain.

2 Material and methods

Figure 1 presents the flowchart of the spatialization process of high-resolution R-410A emissions from the RAC sector in China. This study was based on the prefecture-level R-410A emissions data from the RAC sector from Liu et al. (2019). Proxy factors, including GDP, NTL, heating degree days and cooling degree days (HDD18 & CDD26), RP, and average annual temperature (AAT), were included to develop high-resolution HFC emissions. To minimize the effects of the linear additivity, proxy factors were divided by the area to get the values per unit area. Then, the per unit area values were used in the following analyses as well. Correlation analysis was performed to find the most proper proxy factor. Models, including principal component analysis (PCA), multiple linear regressions, stepwise regressions, and linear regression, were developed to find the one with the best performance. The following parameters, including relative error (RE), root-mean-square error (RMSE), normalized mean bias (NMB), normalized mean error (NME), mean absolute error (MAE), and correlation coefficient (R), were used to evaluate the model

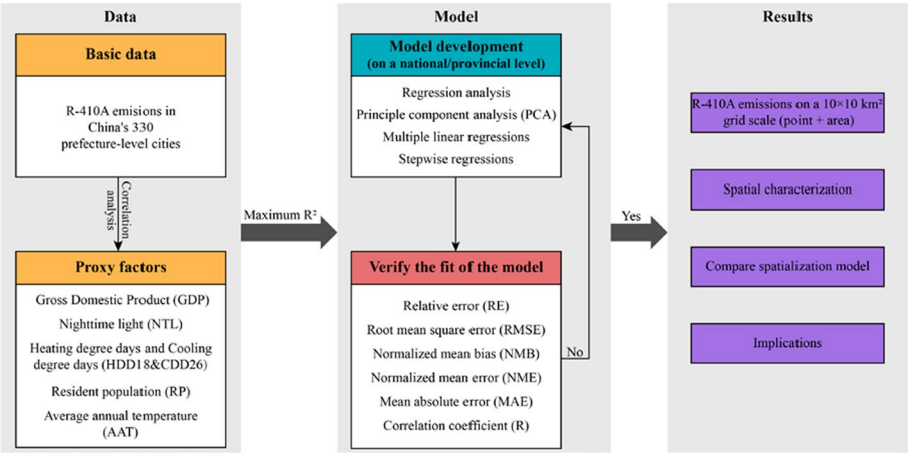

Fig. 1 Flowchart of spatialization of R-410A emissions from the room air-conditioning sector

prediction results, which indirectly support the rationality of our study method. In order to improve the model performance, this study further used regression analysis on a provincial level to spatialize R-410A emissions. Finally, R-410A emissions from the RAC sector in China were spatialized on a 10×10 km^2 grid scale.

2.1 Prefecture-level R-410A emissions inventory from the RAC sector

Prefecture-level R-410A emissions data from the RAC sector were obtained from Liu et al. (2019) and updated to 338 cities, which was based on a bottom-up method. R-410A emissions can be aggregated into five stages of the life cycle, including the production (where air-conditionings (AC) are manufactured, and R-410A is charged), installation (when AC unit is installed for the first time), operation (release into the atmosphere due to leakage during normal operation), servicing (during the servicing of the refrigeration system of AC), and end-of-life emission (during the disposal process).

In the spatialization process, R-410A emissions at the production stage were regarded as point source emissions, which were acquired from manufacturers. The distribution of point sources is shown in Figure S1. R-410A emissions at the other four stages were regarded as area sources based on statistical administrative region border.

2.2 Proxy factors

The selection of proper proxy factors is necessary to conduct the spatialization process. Referring to previous study findings and common practices in the spatialization process (Cai, 2014; Cai et al., 2017; Wang et al., 2014), R-410A emissions from the RAC sector are likely correlated with GDP, RP, AAT, HDD18 & CDD26, and NTL.

Specifically, GDP and RP are the main indicators of human activity, which is directly associated with anthropogenic GHG emissions, including R-410A. In addition, previous studies have found that the outdoor temperature is an important factor affecting air-conditioning use (Liu, 2017; Liu et al., 2020). Degree-days index, such as HDD18 & CDD26, is one of the important meteorological parameters. A higher index value usually indicates a higher level of possibility of usage of air-condition for cooling or heating (U.S. EIA, 2021). Finally, NTL data can indirectly reflect the geographical distribution of population density, economic activity level, and energy consumption (Doll & Pachauri, 2010; Letu et al., 2010, Ma et al., 2012; Zeng et al., 2011; Zhuo et al., 2009).

GDP, AAT, RP, and HDD18 & CDD26 data were obtained from the Resource and Environment Data Cloud Platform compiled by the Institute of Geographic Sciences and Natural Resources Research, Chinese Academy of Sciences (excluding Jiayuguan, Gansu Province; and Sansha, Hainan Province due to missing data) (CAS Institute of Geographic Sciences & Natural Resources Research, 2021). These data have been used in previous studies (Cao et al., 2016; Chen et al., 2019; Xu & Liu, 2014; Xu, 2017a, 2017b). The GDP, AAT, and RP statistics were provided at a resolution of 10×10 km^2, and the HDD18 & CDD26 data were provided at the prefecture level. The NTL data were obtained from Defense Meteorological Satellite Program Operational Linescan System (DMSP-OLS) sensors. The sensors work at night and could detect low-intensity lights from urban constructions and even from small-scale residential areas and traffic (excluding the cities of Ngari, Changdu, Linzhi, Nagqu, Shigatse, and Lhoka in Tibet Province due to missing data). The NTL data were provided at a resolution of 10×10 km^2. After data collection and data processing, a total of 330 China's prefecture-level cities were selected in this study because the

proxy factor data were missing for eight cities. The obtained data were processed in ArcGIS software and ultimately yielded a total of 97,146 space grids on a 10×10 km^2 scale.

2.3 Model development

In the development of the model, we evaluated 20 models, including PCA, multiple linear regressions, stepwise regressions, etc. (S1 of Supplemental Information). The results of these methods are discussed and compared in Tables S1–S15 and Figure S2, and we found linear regression model performs the best.

2.3.1 Correlation analysis

Correlation analysis was conducted between the dependent variable, R-410A emissions from the RAC sector, and five independent variables (GDP, RP, AAT, HDD18 & CDD26, and NTL).

First, based on the administrative region border, data of five independent variables were processed in ArcGIS software and scaled up to the prefecture level of 330 cities in China. Second, a scatter plot matrix was plotted in R software to check the normality of each variable. Then, Spearman's rank correlation test was applied to provide correlation information between R-410A emissions and each of the five independent variables. The Performance Analytics package in R software was used to calculate the correlation coefficients. Also, a stepwise regression of five independent variables was performed to check collinearity and select proper independent variables.

As shown in Table 1, the R between R-410A emissions and GDP was the highest (0.82) among all correlation tests, followed by RP (0.78) and NTL (0.61). AAT (0.44) and HDD18 & CDD26 (−0.36) had poor correlation with R-410A emissions. To avoid the multiple collinearity problem between GDP and RP and between GDP and NTL (correlation coefficients between GDP and RP and between GDP and NTL were 0.82 and 0.81, respectively), we selected GDP as the proxy factor to spatialize R-410A emissions. We also explored other proxy factors, including RP, AAT, and NTL, in the modeling development, and the detailed results could be found in Method 1–20 of S1. The GDP data have been widely used in other fields to identify the drivers of regional agricultural land changes (Cao et al., 2016), explore key drivers of karst rocky desertification (Xu, 2017a), and detect

Table 1 Correlation coefficients among R-410A and the five selected proxy variables

	R-410A	GDP	RP	HDD18 & CDD26	NTL	AAT
R-410A	1***	0.82***	0.78***	−0.36***	0.61***	0.44***
GDP		1	0.82***	−0.21***	0.81***	0.28***
RP			1	−0.29***	0.64***	0.34***
HDD18 & CDD26				1	0.02	−0.93***
NTL					1	0.00
AAT						1

The numbers represent the Spearman correlation coefficients between each of the two variables.

GDP, gross domestic product; RP, resident population; AAT, average annual temperature; HDD18 & CDD26, heating degree days and cooling degree days; NTL, nighttime light

*** represents a p value < 0.001.

the formation mechanism of the spatial pattern of ecological environment quality in China (Chen et al., 2019). The gridded GDP data have also been optimized over many years (Xu & Liu, 2014), resulting in high data credibility.

2.3.2 Regression analysis on a national level

After GDP was selected as the optimal proxy factor, a regression model was developed to test the relationship between R-410A emissions from the RAC sector and GDP on a national level (including all 330 cities), and the results are shown in Fig. 2. The uncertainty of the model prediction was taken at the 95% confidence level (95% CI).

The two variables show a good linear relationship of:

$$Y = 1.421 \times X, \tag{1}$$

where Y is R-410A emissions from the RAC sector (unit, t), and X is GDP (unit, 10^{10} RMB) with R^2 of 0.85. The fitted linear relationship was then applied on each of the 97,146 space grids to obtain the distribution of R-410A emissions on a 10×10 km^2 grid scale.

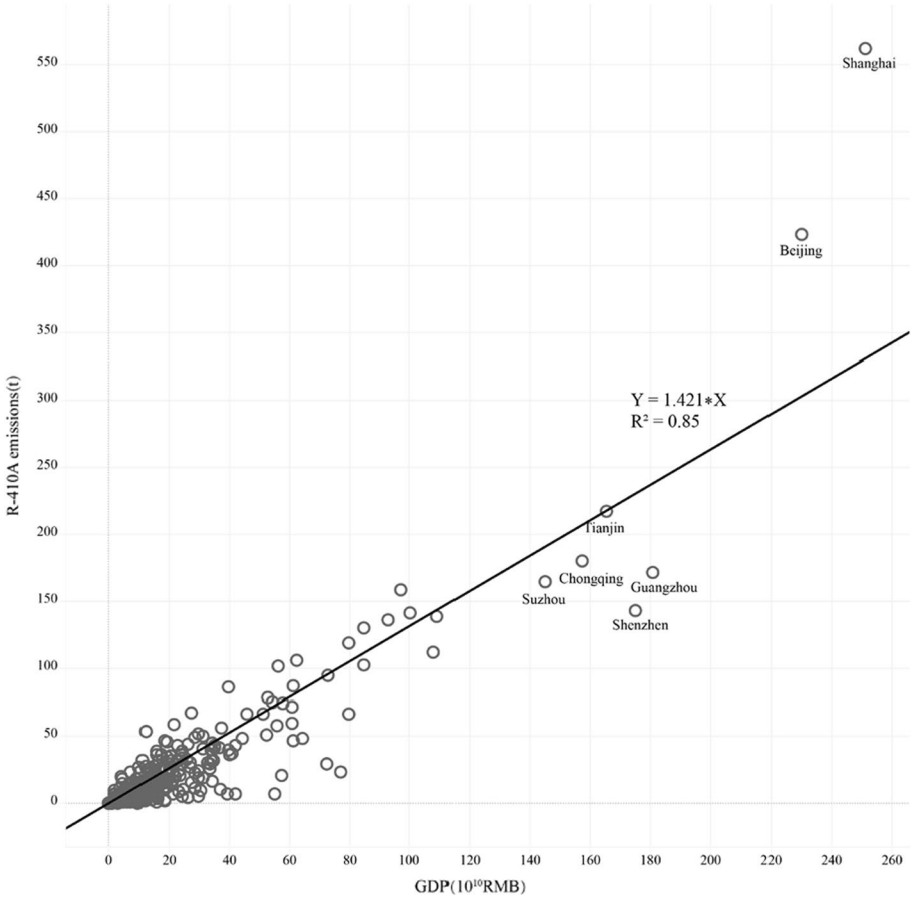

Fig. 2 Linear fitting of GDP and R-410A from the RAC sector in 2015 on a national level

2.3.3 Model evaluation

To test the fit of the spatialization model, the predicted R-410A emissions on a $10 \times 10\ \mathrm{km}^2$ grid scale were aggregated to the prefecture level for 330 cities in China based on the administrative region border. Then, the predicted prefecture-level R-410A emissions are compared with the emission inventory data established by Liu et al. (2019). The following parameters, including RE, RMSE, NMB, NME, MAE, and R, were used to evaluate the performance of the model prediction results:

$$\mathrm{RE} = \frac{(E_{model,i} - E_{Inventory,i})}{E_{Inventory,i}}, \tag{2}$$

$$RMSE = \left[\frac{\sum_{i=1}^{N}(E_{model,i} - E_{Inventory,i})^2}{N}\right]^{1/2}, \tag{3}$$

$$NMB = \frac{\sum_{i=1}^{N}\left(E_{model,i} - E_{Inventory,i}\right)}{\sum_{i=1}^{N} E_{Inventory,i}} \times 100\%, \tag{4}$$

$$NME = \frac{\sum_{i=1}^{N}\left|E_{model,i} - E_{Inventory,i}\right|}{\sum_{i=1}^{N} E_{Inventory,i}} \times 100\%, \tag{5}$$

$$MAE = \frac{\sum_{i=1}^{N}\left|E_{model,i} - E_{Inventory,i}\right|}{N} \tag{6}$$

$$R = \frac{\sum_{i=1}^{N}\left(E_{model,i} - \overline{E_{model}}\right)\left(E_{Inventory,i} - \overline{E_{Inventory}}\right)}{\sqrt{\sum_{i=1}^{N}\left(E_{model,i} - \overline{E_{model}}\right)^2 \sum_{i=1}^{N}\left(E_{Inventory,i} - \overline{E_{Inventory}}\right)^2}} \tag{7}$$

where $E_{model,i}$ is R-410A emissions of the prefecture-level city i from the model prediction, $E_{Inventory,i}$ is R-410A emissions of the prefecture-level city i from emission inventory, $N = 330$, $\overline{E_{model}}$ is the average of the R-410A emissions of the prefecture-level city from the model prediction, and $\overline{E_{Inventory}}$ is the average of R-410A emissions of the prefecture-level city from emission inventory. RE represents the unitless relative deviation between the model prediction value and the emission inventory value for each city; the closer the RE is to zero, the better the prediction performance. RMSE represents the relative deviation between the model prediction value and the emission inventory value for the whole model; the closer the RMSE is to zero, the better the prediction performance. NMB and NME represent the average deviation and the absolute error between the model prediction value and the emission inventory value, respectively. They are both unitless, and the closer they are to zero, the better the prediction performance. MAE is the average of the absolute error between the model prediction value and the emission inventory value, the smaller the value, the better the prediction performance. R is the correlation between

model prediction value and the emission inventory value, the closer R is to 1, the better the prediction performance. It should be noted that in the spatialization of R-410A emissions on a 10 × 10 km^2 grid scale in ArcGIS software, statistical error may occur at the border of a province or city.

2.3.4 Regression analysis on a provincial level

The prediction results from national-level regression analysis in Sect. 2.3.2 and the above model evaluation show that the current model needs improvement (detailed analysis in Sect. 3.2); thus, the regression analysis on a provincial level was used to spatialize R-410A emissions.

For most provinces (no less than 10 city samples), a regression model was developed to test the relationship between R-410A emissions from the RAC sector and GDP on a provincial level. As shown in Fig. 3, the regression results all showed significant linear relationships for each of the provinces. Then, the linear function was applied to each of the space grid within the same province to predict the distribution of R-410A emissions on a 10 × 10 km^2 grid scale. The uncertainty of the model prediction was taken at the 95% CI.

When performing the regression model on provinces without sufficient samples (less than ten city samples), an alternative method was used, including four province-level

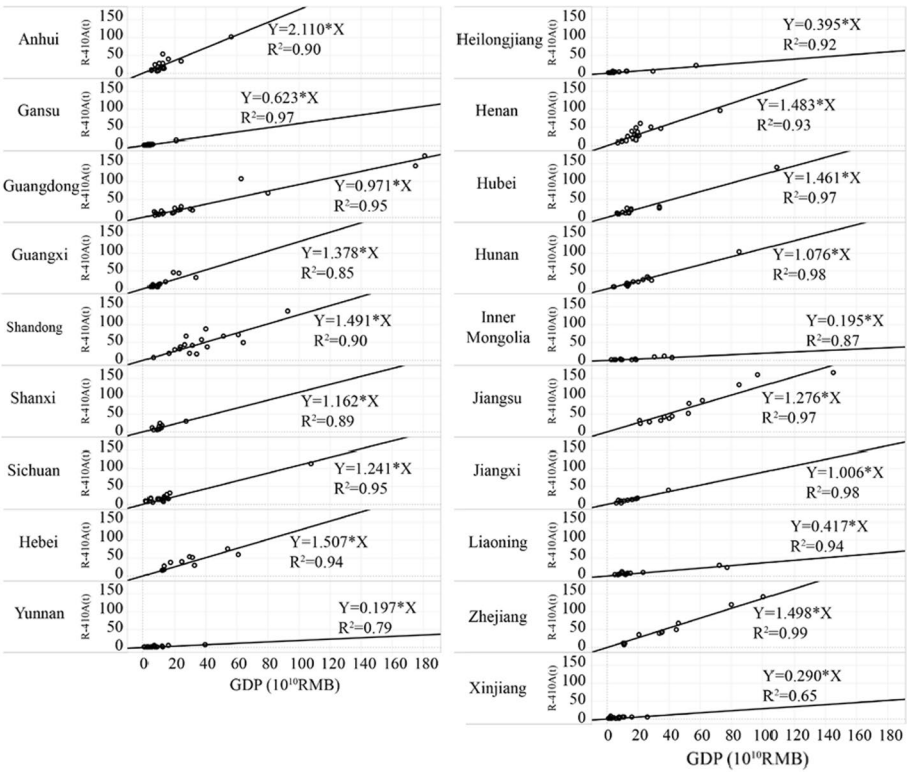

Fig. 3 Linear fitting of GDP and R-410A emissions from RAC in 2015 within each province. Tibet is excluded due to missing data

Fig. 4 **a** R-410A emissions per km^2 from RAC in China in 2015 (modified from Fig. 5 from L. Liu et al., 2019). **b** Spatial distribution of Chinese R-410A emissions from RAC in 2015 by the provincial-level regression analysis (no data available for Hong Kong, Macao and Taiwan in both figures)

municipalities (Beijing, Shanghai, Tianjin, and Chongqing, which only included one data point) and seven provinces (Fujian, Guizhou, Hainan, Jilin, Ningxia, Qinghai, and Shaanxi). Specifically, for each of the province or province-level municipalities, the GDP across all 10 × 10 km^2 grids that was attributed to a province or a province-level municipality was summed, and the original GDP quantity at each grid was normalized by this summed GDP value. The R-410A emissions at a grid were scaled by multiplying the normalized GDP with the annual total R-410A emissions of a province or a province-level municipality, as shown in Eq. (8):

$$R-410A_{grid,j} = \frac{GDP_{grid,j} \times R-410A_{province,j}}{GDP_{province,j}}, \tag{8}$$

where $R-410A_{grid,j}$ (kg) is the R-410A emissions in each of the 10 × 10 km^2 grids of the province or a province-level municipality j, $R-410A_{province,j}$ (kg) is the total R-410A emissions of the province or a province-level municipality j, $GDP_{grid,j}$ (10^{10} RMB) is the GDP value in each of the 10 × 10 km^2 grid of the province or a province-level municipality j, and $GDP_{province,j}$ (10^{10} RMB) is the summed GDP value of the province or a province-level municipality j.

The fit of the model for this provincial-level regression analysis was evaluated using the same parameters as mentioned in Sect. 2.3.3, including RE, RMSE, NMB, and NME.

3 Results and discussion

3.1 The spatial distribution of R-410A emissions from the RAC sector

We used ArcGIS software (version 10) to add point source emissions (production stage) and area source emissions (installing, operation, servicing, and end-of-life stages, which were based on the model predictions from regression analyses in Sect. 2.3.2 or Sect. 2.3.4). The spatial distribution of Chinese R-410A emissions from the RAC sector is shown in Figs. 4 and S3. Figure 4a represents city-level R-410A emissions per km^2 from the existing emission inventory (Liu et al., 2019). Figure 4b represents R-410A emissions per km^2 on a 10 × 10 km^2 grid scale by the provincial-level regression analysis, and Fig. S3 represents R-410A emissions per km^2 on a 10 × 10 km^2 grid scale by the national-level regression analysis.

Compared with the emission inventory data of total R-410A emissions across China, the prediction result using the national-level regression analysis is about 9900 t (95% CI 9455–10,335), which is about 20% higher than the emission inventory value (8200 t) (Liu et al., 2019), while the total R-410A emissions predicted by the provincial-level regression analysis are about 7600 t (95% CI 7391–7868), which is closer to the emission inventory value. Overall, China's R-410A emissions in 2015 show a spatial pattern of high-in-east and low-in-west, with the higher emissions from Beijing-Tianjin-Hebei, the Pearl River Delta, and the Yangtze River Delta regions. The above three regions are characterized by high urbanization and high levels of economic development. Cities with high total

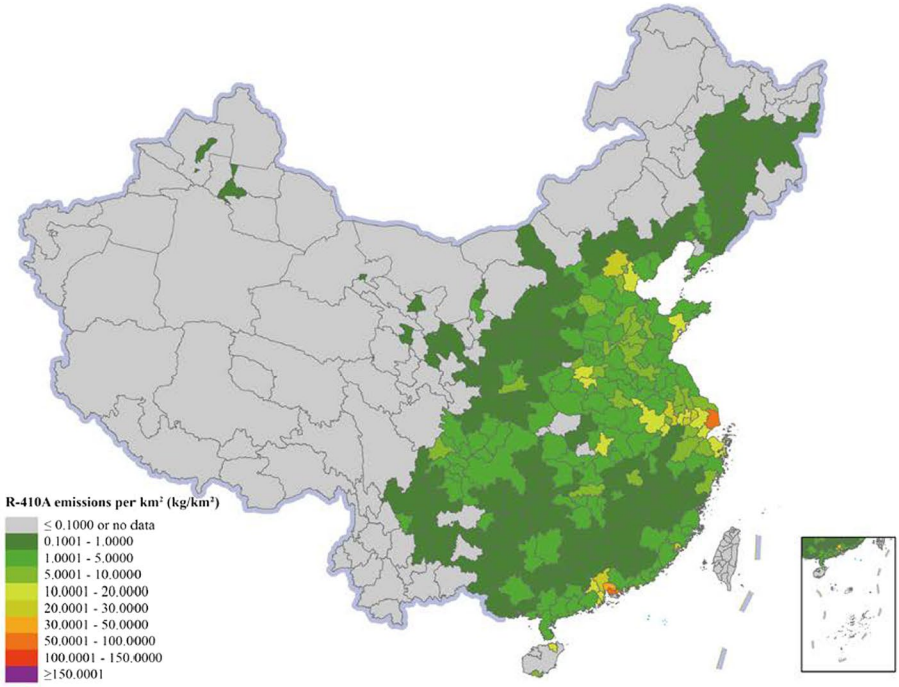
R-410A emissions per km² (kg/km²)
≤ 0.1000 or no data
0.1001 - 1.0000
1.0001 - 5.0000
5.0001 - 10.0000
10.0001 - 20.0000
20.0001 - 30.0000
30.0001 - 50.0000
50.0001 - 100.0000
100.0001 - 150.0000
≥150.0001

(a)

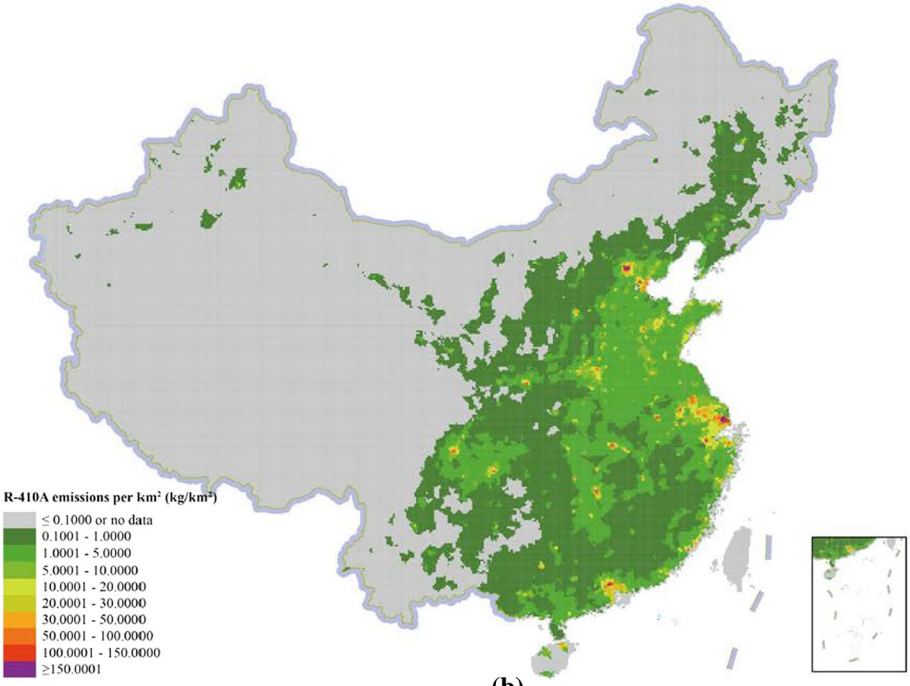
R-410A emissions per km² (kg/km²)
≤ 0.1000 or no data
0.1001 - 1.0000
1.0001 - 5.0000
5.0001 - 10.0000
10.0001 - 20.0000
20.0001 - 30.0000
30.0001 - 50.0000
50.0001 - 100.0000
100.0001 - 150.0000
≥150.0001

(b)

emissions are mainly located in the eastern coastal areas (including Jiangsu, Shandong, Zhejiang, and Guangdong provinces), while cities with lower total emissions are mainly located in the southwest (Yunnan province) and the northeast (including Inner Mongolia and Heilongjiang provinces) areas. Compared with the city-level geographical distribution of R-410A emissions in China in 2015 (shown in Fig. 4a) (Liu et al., 2019), our distribution results show a similar overall spatial pattern. In addition, our study results could provide more detailed information about R-410A emissions in districts and counties or the exact 10×10 km^2 grid.

On the city level, the model prediction by national-level regression analysis (shown in Figure S3) shows higher values in the northeast and western areas, including Yunnan, Xinjiang, Tibet, Qinghai, Jilin, Inner Mongolia, Guizhou, Gansu, Ningxia, Liaoning, and Heilongjiang provinces and lower values in Hainan province, when compared with results from Liu's emission inventory (Liu et al., 2019). However, the cities of Shanghai, Beijing, Guangzhou, Shenzhen, Chongqing, and Suzhou were overestimated or underestimated by the national-level regression analysis, which is likely due to large deviations from the fitted regression line shown in Fig. 2. Regarding the provincial-level regression analysis (shown in Fig. 4b), the model prediction results are higher than emission inventory values in the cities of Xilingol, Alxa League, Chuxiong, and Xuancheng, while lower in cities of Hotan, Dandong, Sanya, and Zhaotong, which could be attributable to the deviations from the fitted regression between GDP and R-410A emissions within the same province. To explore the causes of the differences in spatial distribution between Figs. 4b and S3, we compared the above two analyses quantitatively (shown in Sect. 3.2).

3.2 Model evaluation with emission inventory

To evaluate the fit of the model, the RE was calculated (Eq. (2) in Sect. 2.3.3) to compare the prefecture-level R-410A emissions between the model result and emission inventory, and the frequency distribution of RE is presented in Fig. 5.

In general, RE distribution by the national-level regression analysis does not follow a Gaussian distribution. About 39% of the cities (128 of 330) are within 40% RE, and about

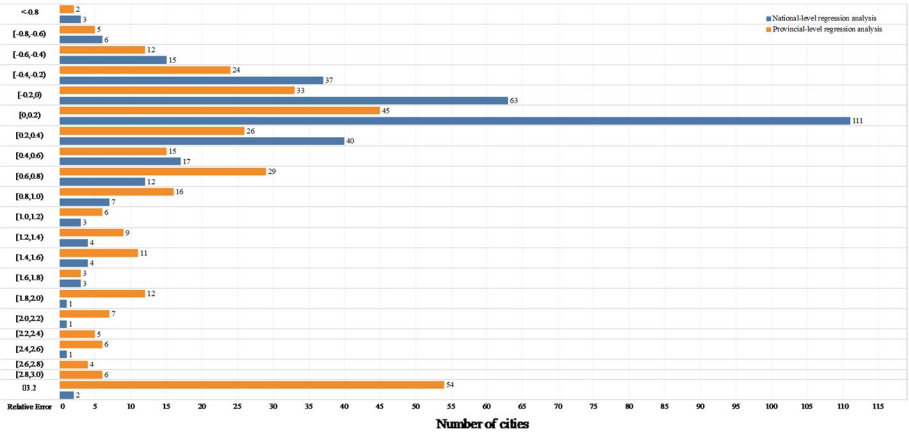

Fig. 5 Frequency distribution of relative error in 330 cities by national-level regression analysis and provincial-level regression analysis in 2015

47% of the cities (155 of 330) are within 60% RE. Previous studies have found that the outdoor temperature is an important factor affecting air-condition use, and there was a strong positive correlation between air-condition use frequency and summer temperature (Liu, 2017; Liu et al., 2020). Most of the provinces in eastern China have high summer temperatures (above 24 °C) and the variation of summer temperatures between these provinces is not obvious. For these provinces, GDP was found as the most correlated proxy factor with R-410A emissions. However, there are still a few provinces with much lower summer temperature (below 24 °C) in China, especially in western or northeast China. In the national-level regression analysis, a linear relationship was developed between GDP and R-410A emissions, which did not take the above influential factor into consideration. Therefore, the R-410A emissions in places with cooler summer temperature are overestimated. Cities with large REs are mainly located in the northeast (Heilongjiang, Jilin, and Liaoning provinces), the west (Xinjiang, Gansu, and Qinghai provinces), Inner Mongolia, and Yunnan Province. Compared to most of the cities in China, average summer temperatures are relatively low for cities with large REs (as shown in Figure S4). Therefore, it could be expected that low summer temperatures are associated with a low frequency of air-conditioner use in these areas.

To account for the influence caused by air-conditioner using behaviors, a regression analysis (Sect. 2.3.4) was developed at the provincial level. Within the same province, the distribution of summer temperature is more uniform than that at the national level, and further, the air-conditioner using behaviors are more similar. Thus, the impact of summer temperature could be minimized. Taking the summer temperature into consideration will optimize the spatialization results of R-410A emissions. Overall, the RE distribution by the provincial-level regression analysis shows a good fit for the normal distribution, with major values concentrated around zero. About 76% of the cities (251 of 330) are within 40% RE, and about 86% of the cities (283 of 330) are within 60% RE. We further extended our analysis in year 2010, and the model evaluation results also show that the model performance of provincial-level regression analysis is better than that of national-level regression analysis (as shown in Figures S6 and S7).

In this provincial-level regression analysis, the coefficients for linear regression analysis are smaller for provinces with low summer temperatures (including Yunnan, Heilongjiang, Inner Mongolia, Liaoning, Xinjiang, and Gansu) compared with most provinces with high summer temperature, which supports the development of our spatialization model from the national level to the provincial level. Besides RE, a comparison of other model evaluation parameters (RMSE, NMB, and NME) between the two analyses is shown in Table 2. The

Table 2 Comparison of model evaluation parameters

Model evaluation parameters (N = 330)	National-level regression analysis	Provincial-level regression analysis
RMSE (t)	20.96	11.35
NMB	0.16	−0.01
NME	0.45	0.20
MAE	11.27	4.97
R	0.91	0.97

RE, abbreviation for relative error; RMSE, root-mean-square error; NMB, normalized mean bias; NME, normalized mean error; MAE, mean absolute error; R, correlation coefficient

RMSE, NMB, and NME values for the provincial-level regression analysis are closer to zero. Based on the above model evaluation results, the provincial-level regression analysis was further improved based on the national-level regression analysis. A similar method was used in previous studies to spatialize emissions of persistent organic pollutant at fine resolution. For example, emissions of α-hexachlorocyclohex were distributed on a 1°×1° longitude and latitude grid scale globally. The gridded cropland data was set as a proxy factor to make the distributions (Li, 1999, 2001; Li et al., 2000), and the results were then aggregated to the country level and compared with the previous emission inventory.

It should be noted that HFC emission could also be derived by a top-down method, which combined atmospheric HFC measurement and inverse modeling. However, the emission by the top-down method was total emission from all sources. Thus, it will not be able to quantify emission from the RAC sector as we did in this study. Although it is difficult to estimate the uncertainty of mapping, we search for evidence that may support our method by some indirect indicators. We have also included the field survey results (showed in Figure S5) conducted at the recycling stations. We further analyzed the relationship between the number of recycling stations and corresponding GDP at the same grid. Major R-410A emissions come from the process of end-of-life emissions, which mainly occurred at recycling stations. However, in China, there was no official statistics on R-410A emissions from recycling stations, thus the number of recycling stations was used instead for statistical analysis, assuming the R-410A emissions were directly proportional to the number of recycling stations. In this study, the key research areas (Beijing, Shanghai, Henan, Hubei, Hunan, Tianjin, Shaanxi, Zhejiang, Jiangxi, and Guangdong) were selected. We used "air-conditioning recycling" and "recycling" as keywords to search the point-of-interest (POI database) of recycling stations on maps and recorded their location information (latitude and longitude), then analyzed the results on the 10×10 km^2 grid. A total of 13,551 recycling points were used in our analysis. As shown in Figure S5, there is a strong correlation between gridded GDP and the number of recycling stations. For example, the correlation coefficients in Beijing, Shanghai, Henan, Hubei, Hunan, Tianjin, Shaanxi, Zhejiang, Jiangxi, and Guangdong are 0.9, 0.8, 0.75, 0.74, 0.72, 0.72, 0.71, 0.7, 0.69, and 0.63, respectively, which indirectly proves the rationality of using GDP as a proxy factor to spatialize R-410A emissions. It is worth mentioning that there may exist some uncertainty and limitations since we only used the number of recycling stations for statistical analysis. Factors such as the size of the recycling station, the way the recycling stations process refrigerant, and the type of room air-conditioning recycled could also affect R-410A emissions.

3.3 Implications

Because of the increasing impact of R-410A on global warming, considering R-410A is a potent GHG with a GWP value of 1923, and the annual R-410A emissions from RAC in China is about 15.4 million t CO_2-eq in 2015 (IPCC, 2013; Liu et al., 2019), developing an accurate and high-resolution emission inventory is important for both the research community and policy makers in reducing GHG. Currently, studies on R-410A emissions from the RAC sector at a high spatial resolution are limited. Previous studies on F-gas emissions used traditional surveys to obtain the activity data and combined them with emission factors to estimate the emissions. However, in some regions and industries, activity levels are difficult or costly to obtain. This study analyzed various regression models and parameters and found that GDP was the most appropriate proxy factor to spatialize R-410A emissions

in the RAC sector in China. The study results improve the resolution of the spatial allocation of R-410A emissions, and further improve the understanding of the identification and implementation of control strategies.

First, the research on gridded R-410A emissions database provides reference method and solid data foundation for China's GHG emission research and site-specific management of low-carbon development. However, in some regions and industries, activity levels are difficult or costly to obtain, making it hard to establish the emission inventory of F-gas at a high-resolution scale (10×10 km^2). Improving the spatial resolution of the F-gas emission using traditional statistical methods needs a large number of investigations and burdens extremely high survey costs. This method developed in this paper could effectively support the establishment of spatial emission grids with acceptable prediction errors. It is innovative to use such proxy factor rather than population to spatialize the emissions as has been done in previous studies, in which HFC emissions are commonly disaggregated into a smaller grid by population density on a national scale (Keller et al., 2012; Stohl et al., 2010; Vollmer et al., 2009; Yao et al., 2019). In addition, it is essential to verify the emission estimations based on the "top-down" method combining atmospheric in-situ measurements and Bayesian inverse modeling (Yao et al., 2019), which has been systematically illustrated in 2019 Refinement to the 2006 IPCC Guidelines for National Greenhouse Gas Inventories (IPCC, 2019).

In addition, most of the HFC emissions from air-conditioning refrigerants occur during the operation and disposal process. The refined spatial pattern demonstrates large variations for disposal sites. For example, a large disposal site is likely to be the highest emissions in the city. In general, the air-conditionings are installed at different times and thus present different emission characteristics. Therefore, on the provincial and city level, a clear understanding of HFC emissions hotspots is beneficial to make targeted management plans, such as regional management, hotspot responsible-person mechanism, which have been proved successful in air pollution prevention and control in Northern China (The Hot Spot Grid Work Promotion Office of Cangzhou City 2019; Zhao, 2018). Specific emission reduction mitigation measures, such as differentiated economic incentives and penalties to avoid unexpected results because of uniform measures, should also be considered. Hotspot management could greatly improve the pertinence and accuracy of environmental enforcement, and thus, site-specific management based on the utilization of hotspots is suitable for the current management system. Hotspots enable accurate identification of high-emission areas or locations, which reduces the technical monitoring cost and management cost. In addition, it helps to evaluate the emission performance in cities or towns. The management of emission areas could be classified into different grades (for example, major and non-major) according to their emissions, and a responsibility system based on hotpots could be established.

Furthermore, our results could be applied to other countries or regions in the spatialization of R-410A emissions and extended by using updated data to depict the distribution. For countries with similar air-conditioner using behaviors, a regression analysis could be developed to depict R-410A emissions on a national or regional level. However, it should be noted that large uncertainties might be introduced when the method is applied to countries with large summer temperature differences or distinct air-condition using behaviors, such as the USA or Chile. If so, a differentiated spatialization method should be applied (similar to Sect. 2.3.2, the provincial-level regression analysis). In generalization of the model, when the air-condition use behavior becomes an important indicator, the choice on area size in this study could spatialize R-410A emissions at a high-resolution scale (10×10 km^2) rather than the traditionally prefecture-level city that is regulated under the

administrative region, where the concept and scale of cities and provinces in China may not be the exact template for other countries or regions. Thus, the new method has great advantages over previous methods in depicting the spatial distribution characteristics of R-410A emissions.

This study showed that the appropriate proxy factor could be used to develop the HFC emissions on a high-resolution scale. The selection of optimal proxy factor is crucial in the model development. Different HFCs may choose different proxy factors according to their characteristics and usages. For example, HFC-134a is mainly used for automobile refrigerants (Fang et al., 2016), HFC-23 is a by-product of HCFC-22 production from fluorine chemical industry (Stanley et al., 2020). However, in the spatialization process, it may be easy or difficult to find the proper proxy factor for different HFCs, which may be a limitation in the high-resolution HFC emission inventory development.

Supplementary Information The online version contains supplementary material available at https://doi.org/10.1007/s10668-022-02264-z.

Acknowledgements This work was supported by the National Key R&D Program of China (Grant No. 2019YFC0214502) and the National Natural Science Foundation of China (Grant No. 72074154 and No. 72174125).

Author contributions PW and LZ performed research, analyzed data, and wrote the paper; BY, YZ, and BC designed research, performed research and provided the part on policy implication; HL and ZX organized the literature review; HY, YD, PW, LL and YR provided and verified the data; LP, LC, XB, and YL organized and formatted the paper.

Data availability The data and material that supporting the findings of this study are available from the corresponding author (Bo Yao) on request.

Declarations

Conflict of interest All authors declare that they have no conflict of interest or financial conflicts to disclose in the outcome of this study.

References

Cai, B. (2014). CO_2 emissions in four urban boundaries of China—Case study of Chongqing. *China Environmental Science, 34*(9), 2439–2448.

Cai, B., Wang, J., Yang, S., Mao, X., & Cao, L. (2017). Carbon dioxide emissions from cities in China based on high resolution emission gridded data. *Chinese Journal of Population Resources and Environment, 15*(1), 58–70. https://doi.org/10.1080/10042857.2017.1286143

Cai, B., & Zhang, L. (2014). Urban CO_2 emissions in China: Spatial boundary and performance comparison. *Energy Policy, 66*, 557–567. https://doi.org/10.1016/j.enpol.2013.10.072

Cao, Q., Wu, J., Tong, D., Zhang, X., Lu, Z., & Si, M. (2016). Drivers of regional agricultural land changes based on spatial autocorrelation in the Pearl River Delta. *Resources Science, 38*(4), 714–727. https://doi.org/10.18402/resci.2016.04.13

CAS Institute of Geographic Sciences and Natural Resources Research. (2021). Resource and Environment Science and Data Center. Retrieved November 7, 2019 from http://www.resdc.cn/.

Chen, W. X., Li, J. F., Zeng, J., Ran, D., & Yang, B. (2019). Spatial heterogeneity and formation mechanism of ecoenvironmental effect of land use change in China. *Geographical Research, 38*(9), 2173–2187.

China Ministry of Ecology and Environment. (2018). China Second Biennial Update Report on Climate Change. Retrieved September 15, 2021 from https://unfccc.int/sites/default/files/resource/China2BUR_English.pdf.

De Matteis, A. (2017). Decomposing the anthropogenic causes of climate change. *Environment, Development and Sustainability, 21*(1), 165–179. https://doi.org/10.1007/S10668-017-0028-4

Doll, C. N. H., & Pachauri, S. (2010). Estimating rural populations without access to electricity in developing countries through night-time light satellite imagery. *Energy Policy, 38*(10), 5661–5670. https://doi.org/10.1016/j.enpol.2010.05.014

Fang, X., Ravishankara, A. R., Velders, G. J. M., Molina, M. J., Su, S., Zhang, J., et al. (2018). Changes in emissions of ozone-depleting substances from China due to implementation of the Montreal protocol. *Environmental Science & Technology, 52*(19), 11359–11366. https://doi.org/10.1021/acs.est.8b01280

Fang, X., Velders, G. J. M., Ravishankara, A. R., Molina, M. J., Hu, J., & Prinn, R. G. (2016). Hydrofluorocarbon (HFC) emissions in china: an inventory for 2005–2013 and projections to 2050. *Environmental Science & Technology, 50*(4), 2027–2034. https://doi.org/10.1021/acs.est.5b04376

Gao, Y., Gao, X., & Zhang, X. (2017). The 2 °C global temperature target and the evolution of the long-term goal of addressing climate change—From the United Nations Framework Convention on Climate Change to the Paris Agreement. *Engineering, 3*(2), 272–278. https://doi.org/10.1016/J.ENG.2017.01.022

IPCC. (2013). *AR5 Climate Change 2013: The Physical Science Basis. Contribution of Working Group I to the Fifth Assessment Report of the Intergovernmental Panel on Climate Change*. *Cambridge University Press*. Cambridge. Retrieved June 29, 2021 from https://www.ipcc.ch/report/ar5/wg1/.

IPCC. (2019). 2019 Refinement to the 2006 IPCC Guidelines for National Greenhouse Gas Inventories. Retrieved December 28, 2020 from https://www.ipcc.ch/report/2019-refinement-to-the-2006-ipcc-guidelines-for-national-greenhouse-gas-inventories/.

Keller, C. A., Hill, M., Vollmer, M. K., Henne, S., Brunner, D., Reimann, S., et al. (2012). European emissions of halogenated greenhouse gases inferred from atmospheric measurements. *Environmental Science & Technology, 46*(1), 217–225. https://doi.org/10.1021/es202453j

Letu, H., Hara, M., Yagi, H., Naoki, K., Tana, G., Nishio, F., & Shuhei, O. (2010). Estimating energy consumption from night-time DMPS/OLS imagery after correcting for saturation effects. *International Journal of Remote Sensing, 31*(16), 4443–4458. https://doi.org/10.1080/01431160903277464

Li, Y. F. (1999). Global gridded technical hexachlorocyclohexane usage inventories using a global cropland as a surrogate. *Journal of Geophysical Research: Atmospheres, 104*(D19), 23785–23797. https://doi.org/10.1029/1999JD900448

Li, Y. F. (2001). Toxaphene in the United States: 1. Usage gridding. *Journal of Geophysical Research: Atmospheres, 106*(16), 17919–17927. https://doi.org/10.1029/2000JD900824

Li, Y. F., Scholtz, M. T., & van Heyst, B. J. (2000). Global gridded emission inventories of α-hexachlorocyclohexane. *Journal of Geophysical Research: Atmospheres, 105*(D5), 6621–6632. https://doi.org/10.1029/1999JD901081

Liu, B. (2017). Analysis of occupant window and air-conditioner behaviour on building's energy consumption. Retrieved January 17, 2020 from http://cdmd.cnki.com.cn/Article/CDMD-10016-1017169677.htm (in Chinese with English Abstract).

Liu, L., Dou, Y., Yao, B., Bie, P., Wang, L., Peng, M., & Hu, J. (2019). Historical and projected HFC-410A emission from room air conditioning sector in China. *Atmospheric Environment, 212*, 194–200. https://doi.org/10.1016/j.atmosenv.2019.05.022

Liu, M., Yan, L., Li, J., Xu, Z., & Du, S. (2020). Analysis of operation schedule of room air conditioners in Chongqing based on data monitoring platform. *Heating Ventilating & Air Conditioning*. Retrieved January 17, 2020 from http://cdmd.cnki.com.cn/Article/CDMD-10611-1018853908.htm (in Chinese with English Abstract).

Liu, X., Zhu, X., Pan, Y., Ma, Y., Li, T., & Chen, S. (2015). Mapping population distribution by integrating night-time light satellite imagery and land-cover data. In *International geoscience and remote sensing symposium (IGARSS)* (Vol. 2015-November, pp. 2186–2189). Institute of Electrical and Electronics Engineers Inc. https://doi.org/10.1109/IGARSS.2015.7326238

Ma, T., Zhou, C., Pei, T., Haynie, S., & Fan, J. (2012). Quantitative estimation of urbanization dynamics using time series of DMSP/OLS nighttime light data: A comparative case study from China's cities. *Remote Sensing of Environment, 124*, 99–107. https://doi.org/10.1016/j.rse.2012.04.018

Oda, T., & Maksyutov, S. (2011). A very high-resolution (1 km × 1 km) global fossil fuel CO_2 emission inventory derived using a point source database and satellite observations of nighttime lights. *Atmospheric Chemistry and Physics, 11*(2), 543–556. https://doi.org/10.5194/acp-11-543-2011

Olivier, J. G., Schure, K. M., & Peters, J. A. H. W. (2018). *Trends in global CO_2 and total greenhouse gas emissions: 2018 report*. *PBL Netherlands Environmental Assessment Agency*. Retrieved November 7, 2019 from https://www.pbl.nl/en/publications/trends-in-global-co2-and-total-greenhouse-gas-emissions-2018-report.

Stanley, K. M., Say, D., Mühle, J., Harth, C. M., Krummel, P. B., Young, D., O'Doherty, S. J., Salameh, P. K., Simmonds, P. G., Weiss, R. F., & Prinn, R. G. (2020). Increase in global emissions of HFC-23 despite near-total expected reductions. *Nature Communications, 11*(1), 1–6. https://doi.org/10.1038/s41467-019-13899-4

Stohl, A., Kim, J., Li, S., O'Doherty, S., Mühle, J., Salameh, P. K., Saito, T., Vollmer, M. K., Wan, D., Weiss, R. F., & Yao, B. (2010). Hydrochlorofluorocarbon and hydrofluorocarbon emissions in East Asia determined by inverse modeling. *Atmospheric Chemistry and Physics, 10*(8), 3545–3560. https://doi.org/10.5194/acp-10-3545-2010

Su, S., Fang, X., Li, L., Wu, J., Zhang, J., Xu, W., & Hu, J. (2015). HFC-134a emissions from mobile air conditioning in China from 1995 to 2030. *Atmospheric Environment, 102*, 122–129. https://doi.org/10.1016/j.atmosenv.2014.11.057

The Hot Spot Grid Work Promotion Office of Cangzhou City. (2019). The integration between the technology and grid management: taking the atmospheric hot grid management in Cangzhou City as an example. *Environment and Sustainable Development, 44*(2), 53–56. https://doi.org/10.19758/j.cnki.issn1673-288x.201902053 (in Chinese).

U.S. EIA. (2021). Degree days. Retrieved April 17, 2021 from https://www.eia.gov/energyexplained/units-and-calculators/degree-days.php.

UNEP. (2016). *The Kigali Amendment (2016): The amendment to the Montreal Protocol agreed by the Twenty-Eighth Meeting of the Parties*. Kigali. Retrieved November 18, 2019 from https://ozone.unep.org/treaties/montreal-protocol/amendments/kigali-amendment-2016-amendment-montreal-protocol-agreed.

UNFCCC. (2015). What is the Paris Agreement? Retrieved November 7, 2019 from https://unfccc.int/process-and-meetings/the-paris-agreement/what-is-the-paris-agreement.

US EPA. (2021). Inventory of U.S. Greenhouse Gas Emissions and Sinks. Retrieved November 7, 2019 from https://www.epa.gov/ghgemissions/inventory-us-greenhouse-gas-emissions-and-sinks.

Velders, G. J. M., Fahey, D. W., Daniel, J. S., Andersen, S. O., & McFarland, M. (2015). Future atmospheric abundances and climate forcings from scenarios of global and regional hydrofluorocarbon (HFC) emissions. *Atmospheric Environment, 123*, 200–209. https://doi.org/10.1016/j.atmosenv.2015.10.071

Velders, G. J. M., Fahey, D. W., Daniel, J. S., McFarland, M., & Andersen, S. O. (2009). The large contribution of projected HFC emissions to future climate forcing. *Proceedings of the National Academy of Sciences of the United States of America, 106*(27), 10949–10954. https://doi.org/10.1073/pnas.0902817106

Vollmer, M. K., Zhou, L. X., Greally, B. R., Henne, S., Yao, B., Reimann, S., et al. (2009). Emissions of ozone-depleting halocarbons from China. *Geophysical Research Letters, 36*(15), L15823. https://doi.org/10.1029/2009GL038659

Wan, D., Xu, J., Zhang, J., Tong, X., & Hu, J. (2009). Historical and projected emissions of major halocarbons in China. *Atmospheric Environment, 43*(36), 5822–5829. https://doi.org/10.1016/j.atmosenv.2009.07.052

Wang, J., Cai, B., Cao, D., Liu, L., Zhou, Y., Zhang, Z., & Xue, W. (2014). China 10km carbon dioxide emissions grid dataset and spatial characteristic analysis. *China Environmental Science, 34*(1), 1–6.

Wang, Z., Fang, X., Li, L., Bie, P., Li, Z., Hu, J., et al. (2016). Historical and projected emissions of HCFC-22 and HFC-410A from China's room air conditioning sector. *Atmospheric Environment, 132*, 30–35. https://doi.org/10.1016/j.atmosenv.2016.02.029

World Meteorological Organization. (2018). *Executive Summary: Scientific Assessment of Ozone Depletion: 2018, Global Ozone Research and Monitoring Project–Report*. Geneva, Switzerland. Retrieved November 7, 2019 from https://www.esrl.noaa.gov/csd/assessments/ozone/2018/executivesummary/.

Xu, E. (2017a). Spatial variation in drivers of karst rocky desertification based on geographically weighted regression model. *Resources Science, 39*(10), 1975–1988. https://doi.org/10.18402/resci.2017.10.16

Xu, X. (2017b). China GDP spatial distribution kilometer grid dataset. *Resource and Environment Data Cloud Platform, Institute of Geographic Sciences and Natural Resources Research, Chinese Academy of Sciences*. https://doi.org/10.12078/2017121102

Xu, X., & Liu, L. (2014). 1 km grid GDP data of China (2005, 2010). *Acta Geographica Sinica, 69*(s1), 45–48.

Yao, B., Fang, X., Vollmer, M. K., Reimann, S., Chen, L., Fang, S., & Prinn, R. G. (2019). China's hydrofluorocarbon emissions for 2011–2017 inferred from atmospheric measurements. *Environmental Science & Technology Letters, 6*(8), 479–486. https://doi.org/10.1021/acs.estlett.9b00319

Yilmaz, V., & Can, Y. (2019). Impact of knowledge, concern and awareness about global warming and global climatic change on environmental behavior. *Environment, Development and Sustainability, 22*(7), 6245–6260. https://doi.org/10.1007/S10668-019-00475-5

Zeng, C., Zhou, Y., Wang, S., Yan, F., & Zhao, Q. (2011). Population spatialization in China based on night-time imagery and land use data. *International Journal of Remote Sensing, 32*(24), 9599–9620. https://doi.org/10.1080/01431161.2011.569581

Zhao, S. (2018). Analysis and enlightenment on atmospheric hot grid construction in Jing-Jin-Ji Region. *Journal of EMCC, 28*(05), 67–69. https://doi.org/10.13358/j.issn.1008-813x.2018.0825.03 (in Chinese).

Zhuo, L., Ichinose, T., Zheng, J., Chen, J., Shi, P. J., & Li, X. (2009). Modelling the population density of China at the pixel level based on DMSP/OLS non-radiance-calibrated night-time light images. *International Journal of Remote Sensing, 30*(4), 1003–1018. https://doi.org/10.1080/01431160802430693

Publisher's Note Springer Nature remains neutral with regard to jurisdictional claims in published maps and institutional affiliations.

Authors and Affiliations

Pengcheng Wu[1,2] · Li Zhang[2,3] · Bo Yao[4] · Bofeng Cai[2] · Yifang Zhu[3] · Hui Liu[5] · Pengling Wang[6] · Lisha Liu[7] · Yanwei Dou[8] · Han Yan[9] · Yijun Liu[10] · Zixuan Xie[11] · Lingyun Pang[2] · Libin Cao[2] · Yimeng Ren[12] · Xin Bo[13]

1 School of Public Health, Sun Yat-Sen University, Guangzhou 510080, Guangdong, China

2 Center for Carbon Neutrality, Chinese Academy of Environmental Planning, Beijing 100012, China

3 Department of Environmental Science and Engineering, Institute of Environment and Sustainability, University of California Los Angeles, Los Angeles, CA 90095, USA

4 Department of Atmospheric and Oceanic Sciences & Institute of Atmospheric Sciences, Fudan University, Songhu Road 2005, Shanghai 200438, China

5 School of Resource and Environmental Sciences, Wuhan University, Wuhan 430072, China

6 National Climate Center, Beijing 100081, China

7 Water Research Center, University of New South Wales, Sydney 2052, Australia

8 China Household Electrical Appliances Association, Beijing 100010, China

9 Taikang Asset Management Co., LTD, Beijing 100033, China

10 School of Environmental Science and Engineering, Shanghai Jiao Tong University, Shanghai 200240, China

11 Department of Energy, Environmental and Chemical Engineering, Washington University in St. Louis, St. Louis, MO 63130, USA

12 School of Statistics, Renmin University of China, Beijing 100872, China

13 Department of Environmental Science and Engineering, Beijing University of Chemical Technology, Beijing 100029, China